Journal of The Electrochemical Society

OPEN ACCESS

Influence of Surface Strain on Passive Film Formation of Duplex Stainless Steel and Its Degradation in Corrosive Environment

To cite this article: Cem Örnek *et al* 2019 *J. Electrochem. Soc.* **166** C3071

JES Focus Issue on Advanced Techniques in Corrosion Science in Memory of Hugh Isaacs

Influence of Surface Strain on Passive Film Formation of Duplex Stainless Steel and Its Degradation in Corrosive Environment

Cem Örnek,[1] Marie Långberg,[1,2] Jonas Evertsson,[3,4,5] Gary Harlow,[3,*] Weronica Linpé,[3] Lisa Rullik,[3] Francesco Carlà,[6] Roberto Felici,[7] Ulf Kivisäkk,[8] Edvin Lundgren,[3] and Jinshan Pan[1,*,z]

[1]*Division of Surface and Corrosion Science, School of Engineering Sciences in Chemistry, Biotechnology and Health, KTH Royal Institute of Technology, SE-100 44 Stockholm, Sweden*
[2]*Swerim, SE-16407 Kista, Sweden*
[3]*Division of Synchrotron Radiation Research, Lund University, SE-221 00 Lund, Sweden*
[4]*Deutsches Elektronen-Synchrotron (DESY), 22607 Hamburg, Germany*
[5]*Physical Chemistry Department, Justus-Liebig-University Giessen, 35392 Giessen, Germany*
[6]*Diamond Light Source, Didcot OX11 0DE, United Kingdom*
[7]*SPINCNR, Area della Ricerca di Roma 2 - Tor Vergata, 00133 Rome, Italy*
[8]*Sandvik Materials Technology, SE-81181 Sandviken, Sweden*

The effect of surface strain on the passive film evolution of SAF 2507 super duplex stainless steel exposed to ambient air and 0.1 M NaCl solution with varying anodic polarization at room temperature has been investigated using in-situ grazing incidence X-ray diffraction (GIXRD) in combination with electrochemical measurements. Surface strain affected the crystallinity of the passive film as such that the surface oxides/hydroxides were predominantly amorphous, with some minor crystalline CrOOH and FeOOH present in the film. Crystalline CrOOH was seen to diminish in volume upon immersion in the NaCl solution, well-possibly becoming amorphous during anodic polarization, whereas crystalline FeOOH was seen to increase in volume during polarization to the passive potential regime. Strain relaxation, associated with metal dissolution, occurred in both austenitic and ferritic grains during immersion in the electrolyte. Anodic polarization to the transpassive regime led to maximum strain relaxation, occurring more on the austenite than the ferrite. The selective transpassive dissolution nature of the ferrite was significantly reduced due to large strains in the austenite. Passive film breakdown was reflected by enhanced dissolution of Fe, Cr, Mo and Ni occurring simultaneously around 1300 mV vs. Ag/AgCl.

 [DOI: 10.1149/2.0101911jes]

Manuscript submitted January 29, 2019; revised manuscript received March 20, 2019. Published April 4, 2019. *This paper is part of the JES Focus Issue on Advanced Techniques in Corrosion Science in Memory of Hugh Isaacs.*

The characterization of the outermost surface of metals has utmost importance as it is the passive film which is in direct contact with the environment and which determines the material's resistance against corrosion.[1–10] Structural as well as chemical information of the surface oxide film in corrosive environments, ideally measured in-situ, is needed to understand its degradation behavior in order to improve our understanding about the initiation and propagation of localized corrosion. So far, there has been an ample amount of research conducted on the passive film of iron and steels, but a fundamental understanding about passive film formation of multi-phase, polycrystalline stainless steels and its degradation in corrosive environment has not been established. The reason is because of the complex nature of oxide formation and the interaction of all compounds in the oxide with the environment.[1–6,8–12] There is, however, agreement that the passive film of stainless steels is usually composed of two distinct layers: an inner barrier layer of Cr-rich oxide/hydroxide and a top-outer layer of Fe-rich oxide/hydroxide, with the film composition changing with depth, and most-likely also along its width.[1,2,4,6,8–13] The exact composition of the passive film depends on the microstructure of the stainless steels and also the environment, with time well-possibly also having influence. Moreover, the thickness of the native passive film is usually between 1–3 nm, and its short- as well as long-range structural order depends on surface aging and environment.[6,8–10,12–15] The native oxide on stainless steels contains usually only Cr(VI) species with Cr(IV) possible to form but not stable after prolonged exposure to air.[9] The structure of the passive film, i.e. whether the oxides/hydroxides are crystalline or amorphous, has remained less understood, although some valuable knowledge about atomistic processes on oxide/hydroxide formation has been established.[1–5,11–19] The air-formed oxide is usually amorphous but becomes crystalline with time, with the alloy composition and the environment playing a decisive role.[20]

Most studies have been performed on pure materials, single crystals, or model alloys, being valuable in understanding passive films, however, having less significance in understanding passive film formation as well as its degradation of commercial alloys, such as duplex stainless steel. In earlier work,[16] the native surface oxide of SAF 2507 super duplex stainless steel, aged for one week in ambient air, was shown to have a nanocrystalline structure and composed of a mixed-oxide containing Cr-, Fe-, Mn-, and Mo-species. It was further demonstrated that the degradation of the passive film in 1 M NaCl solution at room temperature begins with the preferential dissolution of iron primarily from the ferrite lattice. The oxidation of iron was shown to occur when the metal is in its passive regime. Upon anodic polarization to the transpassive regime, the crystallinity of the passive film was reduced due to defect formation in the oxide, resulting in the breakdown of the film and selective dissolution of the ferrite, with less attack occurring on the austenite. The surface film, re-formed after breakdown, was shown to have a different chemical composition, showing a thicker, semi-crystalline, and a more defective nature. This paper is a follow-up work focusing on the effect of surface strain, caused by different sample preparation (grinding and polishing), on the passive film formation and its degradation in a chloride-containing aqueous medium.

Experimental

The material used was SAF 2507 (UNS S32750) super duplex stainless steel from AB Sandvik Materials Technology, with following composition: 24.9% Cr, 6.9% Ni, 3.89% Mo, 0.77% Mn, 0.6% Si, 0.26% Cu, 0.27% N (wt.-%), and other elements. Hat-shaped samples, as shown in Figure 1, were manufactured from the plate material

*Electrochemical Society Member.
zE-mail: jinshanp@kth.se

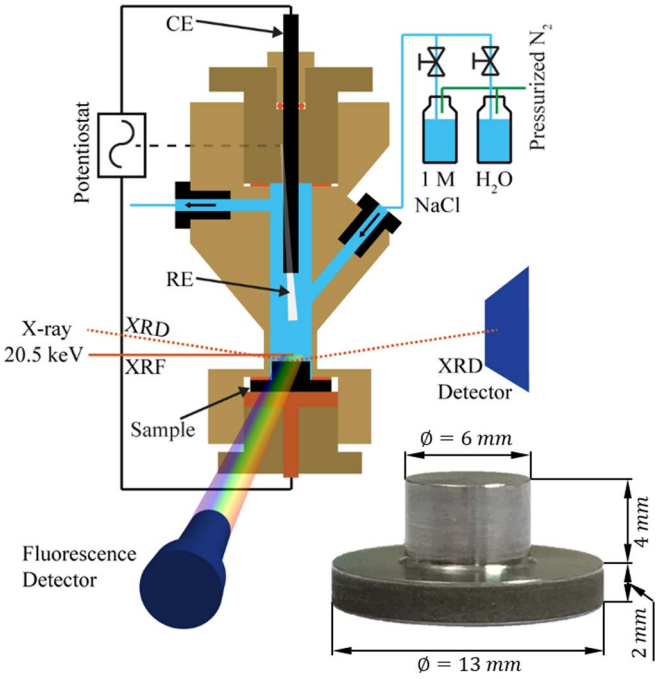

Figure 1. Schematic illustration of the electrochemical cell, made of PEEK, used for in-situ synchrotron X-ray studies. A photograph of the sample used is also shown.

so that the surface was parallel to the normal plane of the plate. The samples were mechanically ground down to 4000-grit size, followed by mirror-polishing using 3, 1, and 1/4 μm diamond paste slurries with deionized water. The samples were flushed with a large stream of deionized water, then dried with blowing air, and then stored in a sample storage box for seven days until the measurement at the synchrotron radiation facility was conducted. In earlier work,[16] the same material and preparation were used except that an extra step for the sample in earlier work was OP-S polished for 16 hours using a Vibromat polisher, followed by a short 1/4 μm polishing to have the same aging and surface end-finish as the sample used in this work. The OP-S suspension (Struers, Denmark) contains active silica colloidal particles in an alkaline solution (pH 9–10), which gently etches the surface during mechanical polishing and removes most surface strains/stresses due to grinding and polishing. The sample used in this work, hence, is significantly more surface-strained than the sample used in earlier work.[16]

GIXRD was used to obtain real-time structural information and to derive chemical information of the passive film formed in ambient air and during exposure to deionized water/ambient air and aqueous 0.1 M NaCl electrolyte at ambient temperature. An electrochemical cell, as shown in Figure 1, was used for the measurements. The cell material was polyether ether ketone (PEEK), which is transparent to x-rays. The cell consisted of an Ag/AgCl (3.5 M KCl) reference electrode and a glassy carbon counter electrode. Electrochemical polarization of the sample was performed at room temperature in 0.1 M NaCl (aq), and the potential was swept up to the transpassive regime in steps beginning at 600 mV, then at 900 mV, 1000 mV, 1100 mV, 1200 mV, 1300 mV, and 1400 mV. All potentials stated in this paper are in reference to Ag/AgCl. The electrochemical current was recorded for 10 minutes at each applied potential, followed by the in-situ XRD measurement at the applied anodic potential (total polarization time at each step was ca. 60 minutes without an XRD and 120 minutes with an XRD measurement). The last XRD measurement, however, was done after the termination of the final polarization step (1400 mV). The volume of the electrolyte in the cell was ca. 3 ml, and new electrolyte was continuously pumped throughout the experiments. Before and after each XRD measurement, chemical analysis of the solution at a position of 3 mm above the sample surface was performed via X-ray fluorescence (XRF) for 1 minute, with the beam shining through the electrolyte parallel to the surface of the sample. The XRF signals were calibrated using metallic elements in the electrolyte with known concentration, and those signals were used for background subtraction for data analysis. Characteristic emission peaks for Fe, Cr, Ni, and Mo were assigned by calibrating the detector channels using a number of reference samples and identifying the measured peaks according to accepted values.[21] The reported XRF signals are not cumulative as new electrolyte was constantly pumped into the cell.

The measurements were performed at the ID03 beamline at the European Synchrotron Radiation Facility (ESRF). The photon energy of the X-rays used was 20.5 keV (λ = 0.6048Å) with a beam size of 90 μm x 35 μm (ellipsoid shape). The X-ray beam impinged on the sample with an incident angle of 1°, and then with an angle of 5°, yielding signals that were more influenced by the sub-surface. The beam size area impinging on the surface (with 1°) was $\sim 8.1 \cdot 10^6$ μm^2 yielding signals from a minimum of 36000 grains from both ferrite and austenite phases (average grain size was ~15 μm). The area was $\sim 3.3 \cdot 10^5$ μm^2 for the incidence angle with 5° yielding signals from a minimum of 1450 grains. DIFFRAC.EVA analysis software (Bruker) was used for XRD data analysis by comparing collected diffraction data with the ICDD reference database. Following PDF card numbers of the indexed phases are reported: 01-074-2386 (CrOOH), 01-074-1877 (FeOOH), 04-016-6641 (austenite, γ), and 00-006-0696 (ferrite, δ). The diffraction positions of the reference phases from the database were marked in the diffractograms, and for the purpose of comparison, the 2-Theta positions were converted to the Bragg angles for Cu-Kα (λ = 1.54056Å).

After termination of the last electrochemical polarization step (1400 mV), the surface was examined by using scanning electron microscopy (SEM) in secondary electron (SE) imaging mode, energy-dispersive X-ray spectroscopy (EDX), and electron backscatter diffraction (EBSD) for phase identification. EBSD phase maps and inverse pole figures (IPF) in Z direction were produced using HKL Channel5 program.

Results and Discussion

Electrochemical behavior.—The current density vs. time recorded during anodic polarization at different potentials are shown in Figure 2. For each polarization step until 1000 mV, the current was decreasing with time, reaching values down to 10^{-4} A/cm^2, indicating passive behavior. The current began to increase when the potential was increased to 1100 mV, indicating the onset of electrochemical events for passivity breakdown. The current further increased with increasing polarization, reaching values up to 10^{-3} A/cm^2, clearly indicating the onset and propagation of transpassive dissolution.

Dissolved elements (XRF).—The XRF measurements showed a minor amount of Fe dissolution already to have occurred upon immersion in the electrolyte at open circuit potential (OCP), as can be seen in Figure 3. The K_α-peak of Fe decreased when the sample was polarized to 600 mV and increased back during polarization to 900 mV. Major Fe oxidation occurred during polarization to 1300 mV, at which oxidation of Ni, Mo, and Cr was also detected. Ni, Mo, and Cr began to dissolve simultaneously at 1300 mV. Similar observations were made by Oblonsky and Ryan who reported no dissolution of Ni and Cr to occur at passive potentials of a stainless steel in sulfuric acid solution.[7] When the sample was polarized to 1400 mV, oxidation of Mo increased excessively, whereas oxidation of Ni did not show any noticeable difference. Ni and Mo underwent less anodic dissolution than Cr, indicating enrichment of Ni and Mo in the surface with significant depletion of Fe and Cr. However, the XRF signals from elements with higher energies (as Ni and Mo) typically attenuate less than those with lower energies (as Cr), which may imply that there was a considerable amount of Cr oxidized but not detected.

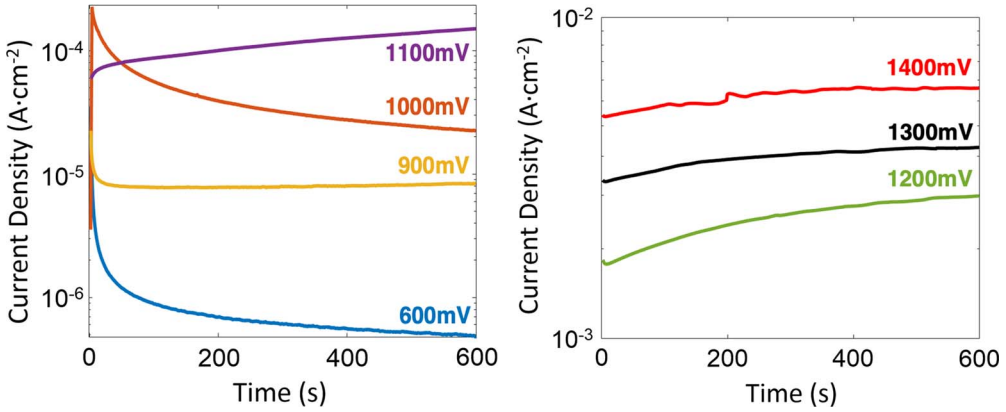

Figure 2. Current transients (in log scale) measured during anodic polarization.

Structure and composition of the outermost surface (GIXRD).— The GIXRD results obtained at an incidence angle of 1° are summarized in Figure 4. Diffraction peaks from ferrite and austenite grains within the scanned 2-theta regime were obtained, yielding five peaks for the austenite and four for the ferrite (Figure 4a). The diffraction pattern, measured in the absence of electrolyte, showed a large background signal, with an increased intensity at lower 2-theta values (tail at the left part) indicating an amorphous structure of the passive film. The results showed scattered data through the entire 2-theta range, supporting this statement. In earlier work, the background signal of the diffraction pattern of the same steel, but without the surface strain (of the same magnitude), was almost zero, and the pattern showed clear, unambiguous diffraction peaks from oxides purporting crystalline structure of the passive film.[16] Apparently, the surface finish had a major effect on the structure of the passive film formed in ambient air. A similar observation was made on an aluminum alloy which showed no selective corrosion behavior in NaCl solution when the surface was polished as contrasted to a state without the mechanically-altered surface, supporting our observations.[22] The passive film on the sample in our work was, however, not entirely amorphous since some small peaks could be unambiguously indexed as crystalline oxy-hydroxides (Figures 4b,4c); three for FeOOH and two

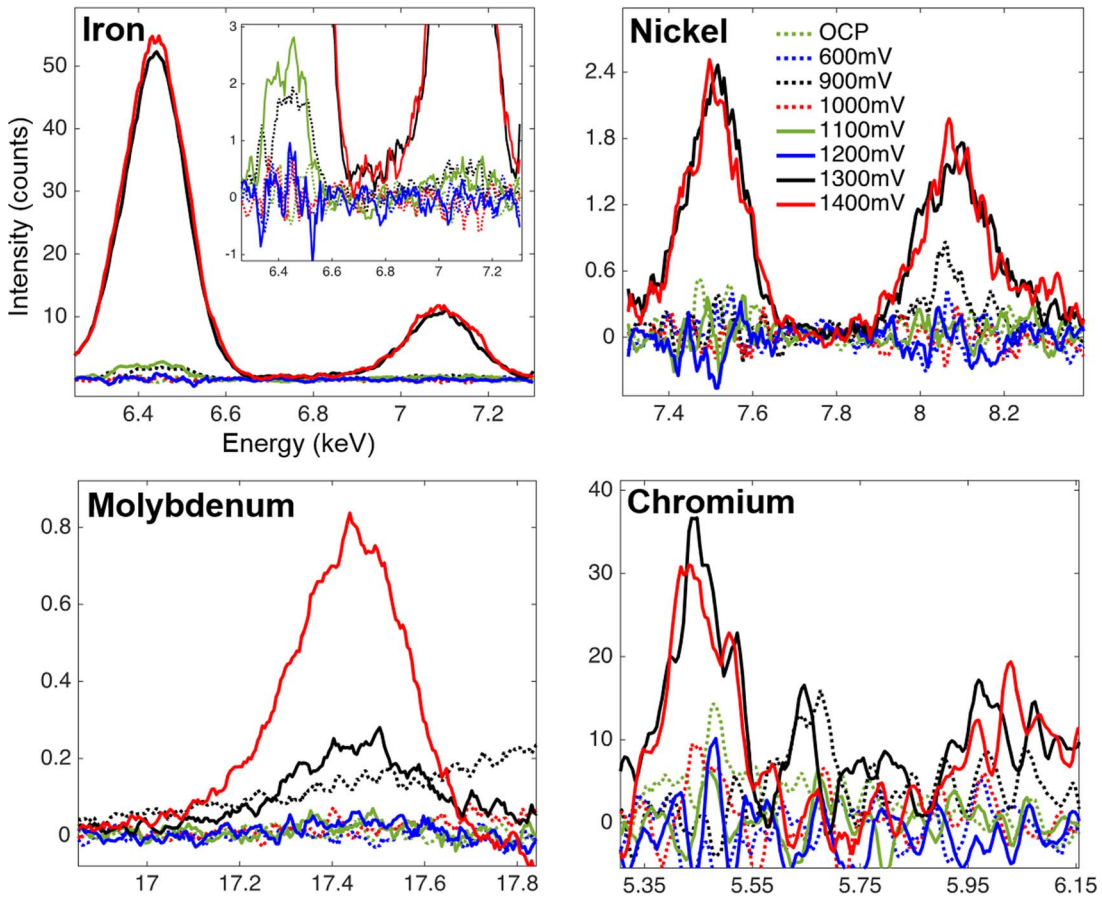

Figure 3. XRF results showing signals for Fe, Ni, Mo, and Cr as a function of anodic polarization. The data are corrected for their cross-sections. The peak of the left hand-side is the Kα-peak.

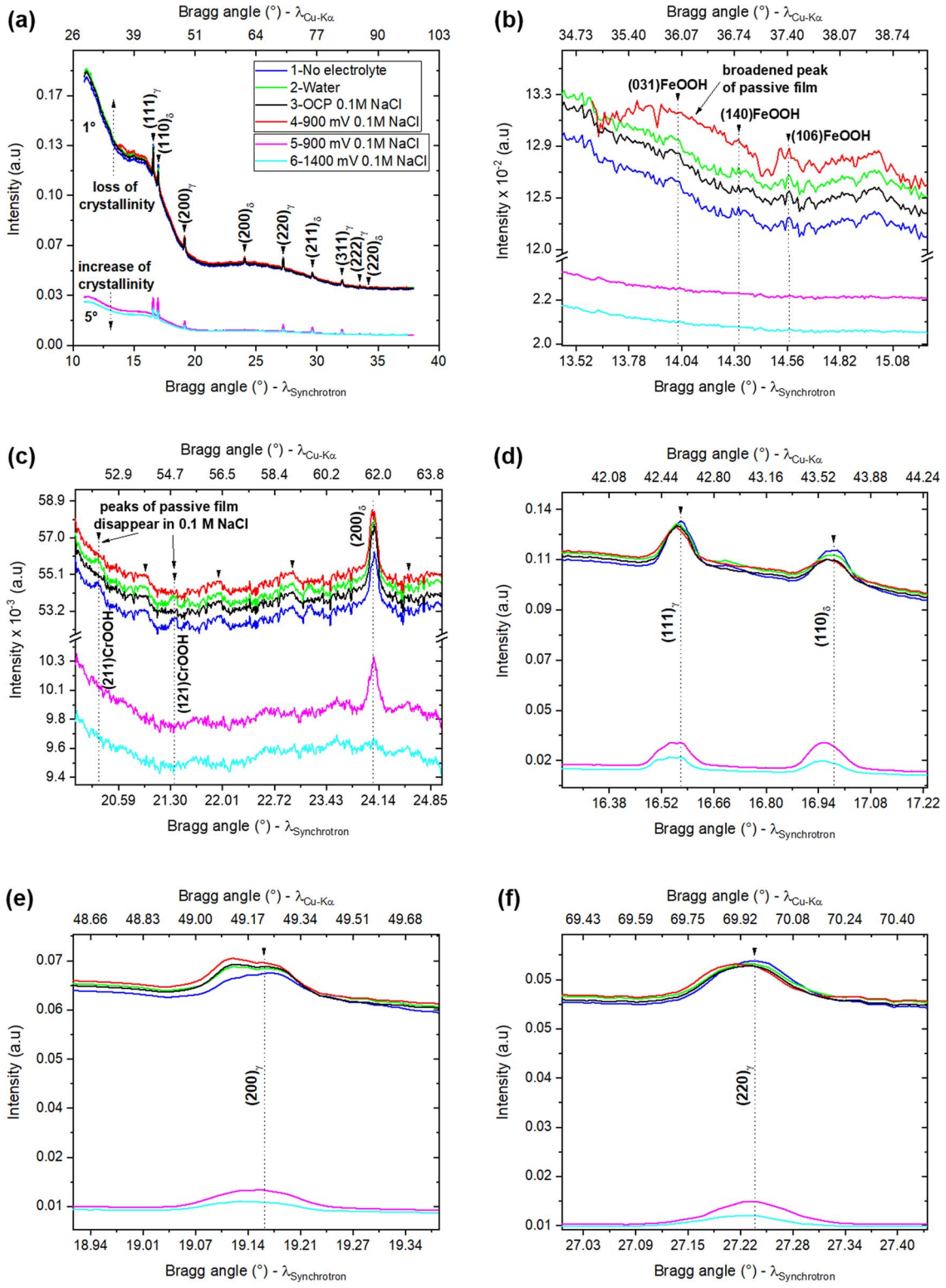

Figure 4. GIXRD results showing (a) the diffraction pattern from the surface with 1° and 5° incidence angle and as a function of anodic polarization, (b) showing increasing peak intensity and peak broadening indicating oxide growth of FeOOH, (c) disappearing peaks for CrOOH and for ferrite due to exposure to 0.1 M NaCl solution and selective dissolution, respectively, (d-f) showing peak shift, peak morphology change and peak intensity reduction of ferrite and austenite peaks.

for CrOOH. Peak broadening was observed indicating polycrystalline morphology showing oxide growth with random orientation. Other small diffraction peaks were also seen, which however could not be associated with any phase/compound.

When deionized water was added to the electrochemical cell, the background signal intensity slightly increased, possibly due to the dissolution of the crystalline hydroxide species formed in ambient air that are soluble in water, or due to the formation of new oxides/

hydroxides on the surface having amorphous character. It is likely that both processes occurred since there is always a competition between oxide formation and dissolution occurring on metal surfaces in aqueous media.[17,18] Alternatively, phase transformation of crystalline to amorphous species may also have occurred which also cannot be ruled out. The diffraction peaks for crystalline FeOOH and CrOOH remained and showed the same intensity, and the un-identified oxide/hydroxide peaks also remained unchanged. Upon exposure to 0.1 M NaCl solution at open-circuit potential, the peaks of all indexed oxides/hydroxides remained unchanged, whereas the background signal decreased, indicating an increase of crystallinity and/or loss of the amorphous part of the passive film. It is likely that the chloride ions at this concentration level caused dissolution of soluble amorphous species without damaging the crystalline oxides/hydroxides formed on the super duplex stainless steel. Chloride absorption into the outer layer of the passive film was shown by *Sato* who also demonstrated that below the repassivation potential of the alloy in a given environment, the chloride at low concentrations contributes to an improved passive behavior.[19]

Polarization to 900 mV vs. Ag/AgCl (3.5 M KCl) increased again the background signal, indicating loss of crystallinity. The intensity of the diffraction peaks as well as their widths for FeOOH increased, clearly indicating oxide growth (Figure 4b). The peaks for the (031)- and (140)-orientations became overlapped. This indicates that the new oxide was nano-crystalline as widened peaks over broad 2-Theta ranges are typical for grain refinement. The peak width/intensity of the (106)-plane also increased, supporting this statement. The anodic oxide growth coefficient is usually 1–2 nm/V for metals such as Fe, Cr and Ni.[23] Here, the oxide growth of FeOOH occurred simultaneously with the dissolution of Fe as detected by XRF. In contrast, the peaks for CrOOH disappeared, indicating dissolution and/or changing to an amorphous compound. No Cr was detected by XRF, suggesting the latter as more likely to have occurred. It is well-likely that CrOOH became amorphous due to vacancy formation as the dissolution of chromium oxy-hydroxides below the transpassive breakdown has not been reported, to the knowledge of the authors at least. However, the dissolution of CrOOH cannot be ruled out as the sensitivity of XRF to Cr is lower than for other elements. In general, hydroxides of Cr are more soluble than those of Fe, and their solubility largely depends on the pH of the solution.[24] The NaCl solution was prepared using deionized water; however, the pH of the chloride solution usually drops down to 5.5 due to dissolution and dissociation of the CO_2 present in the air. Under polarization at high anodic potentials, the pH of the solution near the sample surface can further decrease due to hydrolysis of dissolved metal ions (see Figure 3). This might be the reason for the oxidation of CrOOH, if any, at high potentials. However, it has been reported by Sass and Rai that oxidized chromium-(III) ions have the affinity to co-precipitate with ferric ions as a mixed hydroxide with the formula $Cr_xFe_{1-x}(OH)_3$ due to their similar ionic radii.[24] The mixed hydroxide has been reported to be amorphous, with lower solubility than its own hydroxide species.[24] The GIXRD results in our work did not reveal any new diffraction peak, which may suggest that a similar oxide, as reported by Sass and Rai,[24] was formed onto the surface. The passive films of stainless steels have been commonly reported to consist of a Cr-rich inner layer and a Fe-rich outer layer.[1,2] In this observation, crystalline CrOOH disappeared whereas crystalline FeOOH remained in the passive film at 900 mV. XRF did not detect Cr from oxidized CrOOH, which may indicate that there is no or negligible Cr dissolution into the solution at this potential. Most likely, the crystalline CrOOH became amorphous due to the generation of a large number of vacancies in the lattice, in line with the point defect model,[17,18] although minor amount Cr ions may have migrated through the oxide and hence dissolved into the electrolyte. These observations suggest, furthermore, that most oxidized Fe (detected by XRF) came from the bulk, and that the Fe ions migrated through the oxides/hydroxides (vacancy positions) and perturbed the lattice structure causing strain evolution/relaxation. The latter may also be an explanation for the increase of the background signal since point defects and partial ordering in the surface layer can give rise to low-intensity scattering between the Bragg peaks (diffuse scattering). It should be noted that the passive film was not only composed of crystalline CrOOH and FeOOH but also of amorphous oxides that most-likely accounted for more of the total than the crystalline oxide. An amorphous halo (large background) was seen in the XRD patterns which is a clear sign for amorphous structures in the outermost surface, evidently oxides/hydroxides, which supports this statement. Hence, it is highly speculated that amorphous Cr_2O_3 and Fe_2O_3 formed the major oxide. It is furthermore likely that Cr_2O_3 and Fe_2O_3 are not pure but rather mixed oxides as the investigated duplex stainless steel is highly alloyed. The Cr_2O_3 can contain high levels of Fe and the Fe_2O_3 can be highly rich in Cr, which in both cases can largely shift the characteristic Bragg angles and hence complicate indexing via XRD. We believe that both Fe_2O_3 and Cr_2O_3 existed but were highly amorphous, which seemingly formed the major part of the oxide since a large halo was observed.

Table I. Comparison of peak positions of the indexed crystallographic planes from the strained sample (shown in this paper) and from the non-strained specimen (reported in earlier study[16]).

	2-Theta Position (°)	
Orientation	Sample with more surface strain (this work)	Sample with less surface strain (previous work)
(111)γ	16.57	16.62
(110)δ	16.99	17.01
(200)γ	19.17	19.23
(200)δ	24.08	24.19
(220)γ	27.23	27.33
(211)δ	29.63	29.74
(311)γ	32.07	32.19
(222)γ	33.52	33.65
(220)δ	34.36	34.47

Preferential dissolution (de-alloying) and strain relaxation.— The ratio of the peak intensities to the background signal was relatively low as contrasted to the measurement results on the sample reported in the previous study (sample there had less surface strain).[16] This indicates that strain and/or the presence of amorphous oxide/hydroxide must have led to fewer signals originating from the bulk phases. Furthermore, the diffraction peaks of austenite and ferrite were distorted and broad indicating large strain, as contrasted to the sample reported in earlier work having less/no surface finishing-induced strain due to the final OPS-polishing.[16] Peak broadening is a clear sign of micro-strain (non-uniform) in the microstructure due to crystal defects (dislocations) and/or decrease of the grain size which is also related to defects, i.e. grain boundaries. The latter is less likely to have occurred due to grinding and polishing but may still have been possible as deformation can significantly increase the density of dislocations, which can result in the formation of new (sub)grain boundaries and hence reduce the size of (sub)grains. Kempf et al. reported plastic strain evolution associated with thermal oxide formation on the outermost surface of duplex stainless steel, supporting the observations in this work.[25] Microplasticity was observed occurring more readily on the austenite due to lower yield point, confirming the large propensity for strain evolution due to oxide formation in duplex stainless steel.[25] Kempf et al., furthermore, showed that the duplex microstructure contains large strain gradients, even within single grains.[25] Compressive and tensile strains were seen to co-exist within the same grain showing the complexity of polycrystalline, multi-phase steels.[25]

The peaks indexed in this study were compared with those reported in earlier work, as seen in Table I. The peaks were more distorted indicating a more strained surface, which is assumed to be due to the sample polishing procedure used in this work. The peaks had lower 2-theta positions indicating uniform compressive macro-strains, more in the

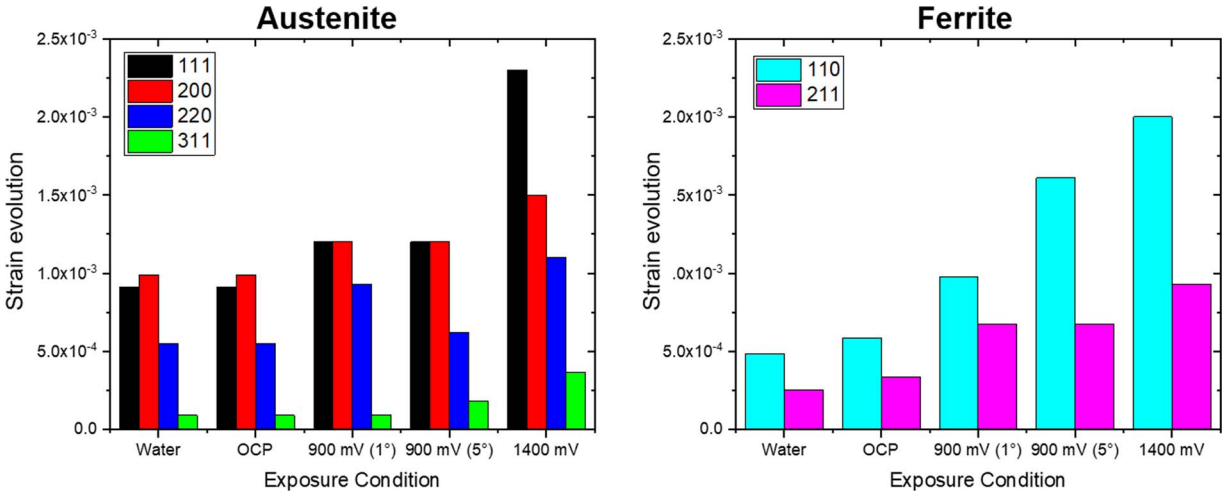

Figure 5. Strain evolution/relaxation in austenite and ferrite grains as a function of exposure conditions. Note that at 900 mV the grazing incidence angle was increased from 1° to 5°.

austenite than in the ferrite. In the approximation of the elastic continuum within the crystalline 'surface', all atoms are shifted due to strain, resulting in changes in the d-spacing. It should be noted that the strain obtained via the GIXRD approach is an average of the x-ray-interacted volume only. Grinding and polishing introduce typically compressive strains into the surface, this, however, toward the depth (stress acting in the z-direction is compressive).[26] The in-plane strain along the surface in lateral dimensions may more likely be tensile due to highly distorted grains[a] on the surface (the average stress is still compressive). Hence, the austenite was more strained both toward the surface and depth due to having more active slip systems facilitating deformation, in line with previous observations.[27–29] Besides, the distorted peaks could be due to an asymmetric distribution of alloying elements, especially nitrogen that is interstitially dissolved in the lattice, causing micro-strain. Thus, strain apparently affected crystal oxide formation and hence the nature of the native passive film. The amorphous nature of the oxide implies that the atoms do not show translation properties and, hence, symmetry relationships as they do in crystalline structures. Amorphous oxides do not have grain boundaries as crystalline oxides. Amorphous oxides have isotropic properties and contain more stored energy. Furthermore, amorphous oxides in the passive film are less dense, which means that localized corrosion events occur in a rather stochastic manner than being deterministic in crystalline passive films. The (defect) structure of amorphous oxides over distance varies less than it does for crystalline oxides (long-range order), hence, chinks in the oxide film are rather uniform when its structure is amorphous, and amorphous passive films are more defective as contrasted to crystalline oxide films.

Dissolution of the surface layer (GIXRD with an incidence angle of 5°).—Increasing the incidence angle to 5° significantly reduced the background signal due to signals emanating from far deeper surface (Figure 4) due to the reduction of scattering volume containing the amorphous phases, approximately five-times more in-depth than the previous setup (incidence angle of 1°). The signal contribution from the oxide diminished to such extent that the signals became less discernible. The background signal further decreased when the sample was polarized to 1400 mV where transpassive dissolution of the passive film and the ferritic and austenitic grains occurred. In earlier work, it was demonstrated that the oxide film dissolved at this potential.[16] This indicates that the reformed oxide was more crystalline than before, clearly demonstrating the effect of strain on passive film formation, since strain relaxation must have occurred during dissolution (oxidation), allowing the growth of new oxides/hydroxides with crystalline structures. In post-exposure surface examination by SEM/EBSD (Figure 6), almost the entire surface could be indexed by EBSD, indicating that the surface strains were largely removed (otherwise the indexing would not have been possible). This observation demonstrates that the super duplex stainless steel has the ability to form crystalline oxides, with the strain clearly affecting the crystallization process. The extent of strain relaxation was calculated relative to the initial surface condition before the exposure to water/electrolyte, as shown in Figure 5. Most strain relaxation occurred on the austenite under all exposure/polarization conditions. The GIXRD results revealed the changes of the ferrite and austenite grains upon dissolution, mostly occurring on (110)-oriented ferritic and (111)-oriented austenitic grains (Figures 4d–4f), with the austenite being less dissolved than the ferrite. The (200) and (220) ferrite faces remained unchanged through the entire exposure conditions, clearly showing that ferrite was less strained than austenite, which is in-line with previous works.[27,28] The strained austenite had a higher susceptibility to metal dissolution than the condition with no/minor surface strain (previous work[16]). This clearly demonstrates that strain accelerates oxidation, with the austenite being more affected than the ferrite due to that fact that the austenite was more strained.

Another observation of the effect of strain on metal oxidation was that the surface oxide was not entirely removed after the termination of the electrochemical polarization (final step was 1400 mV). The diffraction peak shapes remained asymmetric, indicating that the strain-affected layer[b] was not entirely dissolved. The final polishing step was 1/4 μm corresponding to a deformation layer of approximately 125 nm,[30,31] being compressive in nature.[26] The austenite was most strained and therefore highest strain relaxation occurred due to metal dissolution. Apparently, the strain facilitated metal dissolution. Dissolution of ferrite[c] was, however, slightly more enhanced by the polarization as apparent from reduction of peak signals and disappearing signals (Figures 4a, 4c, 4d), also confirmed by post-exposure surface examination by SEM/EBSD (Figure 6) showing more indexed austenite as the ferrite was more dissolved and became recessed in the microstructure due to transpassive dissolution.[d] However, in earlier work,[16] the selective dissolution of the ferrite in the same material was observed, which shows that

[a]The grains are heavily deformed along the surface due to the 'dragging' effect of the grinding/polishing procedure.

[b]It should be noted that the strain-affected layer is thicker than the deformation layer induced by grinding and polishing due to the fact that the deformation layer is compressive in nature and that there is need for stress balance which develops tensile strains beneath the deformation of, perhaps, the same or similar thickness.

[c]The ferrite is also heavily deformed but less than the austenite.

[d]The phase fraction of the microstructure was around 50:50.

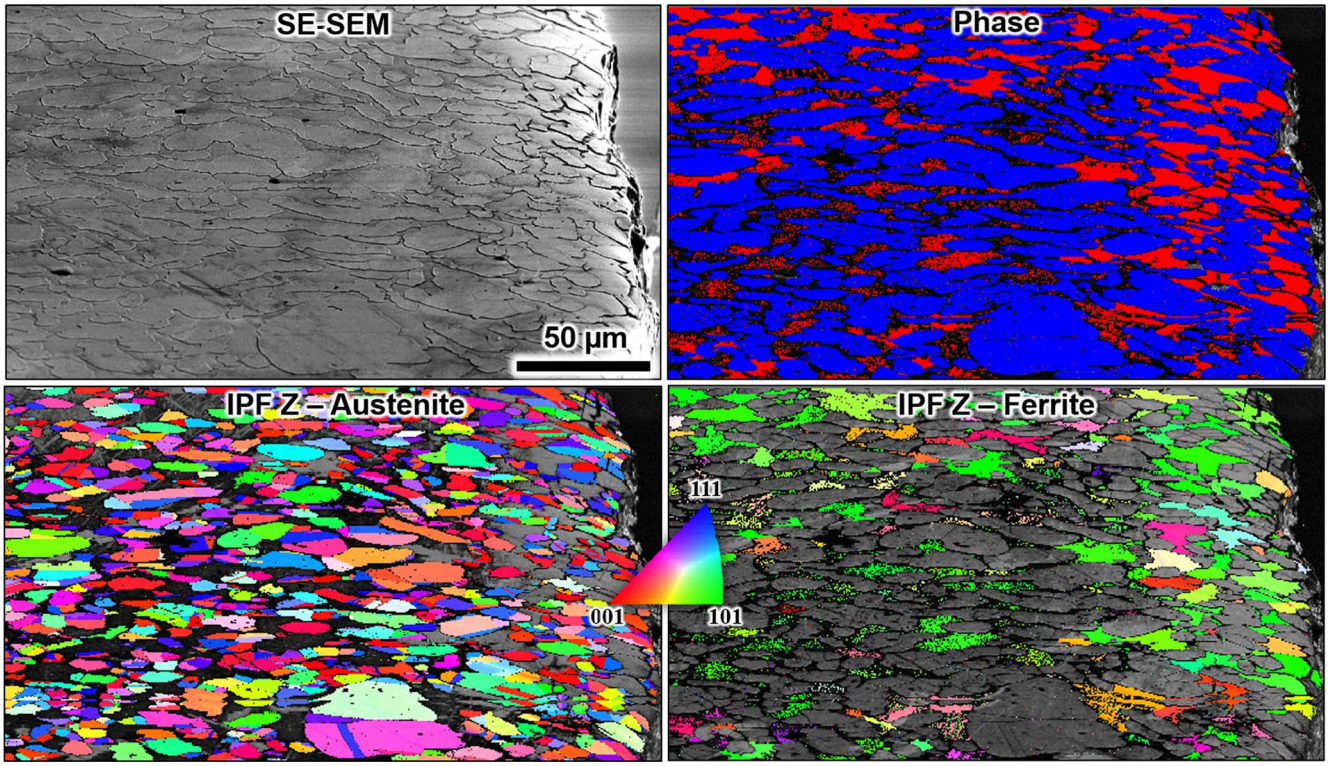

Figure 6. SEM-EBSD analysis of the surface after polarization to 1400 mV in 0.1 M NaCl showing selective dissolution occurred on ferrite with most attack occurring on (101) family planes with least attack happening on (111) family grains. The analysis was performed on the edge of the specimen where most attack occurred.

strain resulted in enhanced dissolution of the austenite, resulting in reduced galvanic coupling between austenite and ferrite. Hence, the dissolution kinetics for the ferrite was decreased, but austenite was still the less dissolving phase. The EBSD analysis further revealed that the dissolution of ferrite was related to crystallographic orientations, with (101)-family grains showing most dissolution (indexing by EBSD was possible). Dissolution of austenite, in contrast, seemed to occur homogeneously in an anisotropic manner. Strain, thus, not only enhanced dissolution but also changed the transpassive dissolution morphology from selective dissolution of ferrite to uniform dissolution of the entire microstructure (Figure 6). In a nutshell, the dissolution of the ferrite was more pronounced upon increasing the anodic potential indicating that the dissolution is polarization-induced, whilst dissolution of the austenite was strain-induced (provoked by polarization) apparent from the reduced selective dissolution nature of the ferrite.

Most transpassive dissolution occurred on the edge of the specimen, with the ferrite being slightly more dissolved than the austenite, apparent from recessed ferrite and higher EBSD band detection rates obtained. The dissolution of the edge and the near-edge regions resembled a more uniform attack, as shown in Figure 6. However, toward the center of the specimen, numerous micro- and nano-pits were observed in both ferrite and austenite grains (Figure 7). The smallest pit observed had a width in the order of 10–20 nm. The pits formed in the austenite were smaller than those formed in the ferrite. These small pits are most-likely associated with local strain pockets (strain localization), earlier introduced as 'hot spots' in the microstructure, which promote accelerated corrosion by the development of numerous micro-galvanic cells.[32] The electron channeling contrast pattern in the SEM images (Figures 7a, 7b) show numerous strain localization sites, with the austenite clearly being more strained than the ferrite. It should be noted that, however, strain localization in duplex stainless steel microstructures does not necessarily indicate stress localization due to the different deformation nature of ferrite and austenite. Despite the higher strains in the austenite, the ferrite is usually more stressed as demonstrated in earlier work.[28]

Near the edge of the sample (further toward the center by 50–200 µm from the position reported above), deposits of corrosion products were seen almost entirely on austenitic sites, indicating that the austenite was nobler than the ferrite, in-line with previous studies.[27,28,32–38] EDX mapping over such areas showed that the corrosion products were primarily composed of Cr and O, with a minor amount of Fe (Figure 8), suggesting chromium oxide/hydroxide. Moreover, stronger oxygen signals were detected on the ferrite, indicating the presence of oxides/hydroxides, which were more readily formed over ferritic sites. This indicates that for the reformed passive film after transpassive dissolution, the oxide composition of the ferrite significantly differs from that of the austenite. EDX mapping further revealed that Cr was not enriched in the ferrite anymore, indicating enhanced Cr dissolution of the ferrite that occurred during transpassive dissolution, resulting in the same/similar Cr composition over austenitic and ferritic sites (Figure 8, Figure 9). Typically, the ferrite has 3–5 wt.-% higher content of Cr than the austenite, whereas Ni is enriched in the austenite (Figure 8 does not show contrast for Cr between the two phases).[39] The EDX analyses were performed with an accelerating voltage of 5 kV which produces an interacting volume of ca. ∼200 nm (the contrast between of Cr signals between ferrite and austenite reduced). It seems that, during transpassive dissolution, the surface became depleted in Cr, resulting in similar contents of Cr for both phases. However, Ni was still enriched in the austenite (Figure 8). Ni was absent in the oxide or had far low concentrations as compared to Cr and Fe, which imply that Ni oxidized significantly less than Cr. Ni is typically enriched beneath the passive film and is known to form the so-called 'surface alloy layer'.[40,41] The strong passive nature of duplex stainless steel is provided by the synergy between the surface oxide film and the underlying Ni-rich layer, retarding metal dissolution. The Ni in the austenite seemingly led to less oxide/hydroxide formation. The surface alloy layer was shown to have a thickness of ∼5 nm in

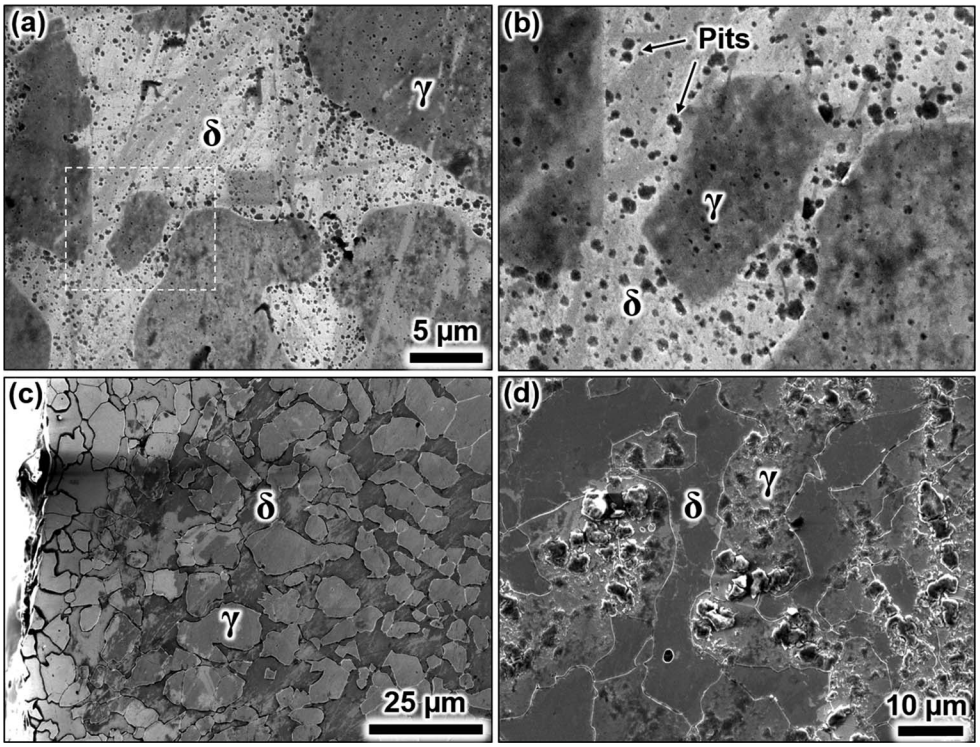

Figure 7. SEM analysis of the surface after polarization to 1400 mV in 0.1 M NaCl showing (a-b) transpassive pitting attack observed at sites between the center and the new-edge of the sample, (c) selective dissolution of the ferrite with less dissolution occurred on the austenite on the edge of the sample, (d) corrosion products deposited almost entirely on austenitic grains.

austenitic stainless steels.[40,42,43] However, the EDX results in this work suggest that the alloy surface layer has a varying thickness across ferrite and austenite regions. The fact that the usual Cr contrast between ferrite and austenite was reduced (see Figure 9) suggests similar Cr-content in the surface layer on the ferrite and austenite. Ni became more enriched in the surface, in particular on austenitic sites. Hence, the ferrite dissolved more Ni than the austenite did, corroborating the statement that most dissolution of the alloying elements occurred from the ferrite. Moreover, the Mo map showed that Mo was still enriched in the ferrite after the transpassive dissolution, indicating a stronger resistance to dissolution.

Transpassive dissolution of the super duplex stainless steel did not occur homogeneously over the surface of the sample as confirmed by post-polarization examinations. Not only the selective dissolution of the phases but also site-specific dissolution kinetics was observed by the SEM/EDX analyses. Figure 9 shows an exposed region close to the edge of the specimen where the chemical contrast between ferrite and austenite was clearly distinguishable. Here, the ferrite was more

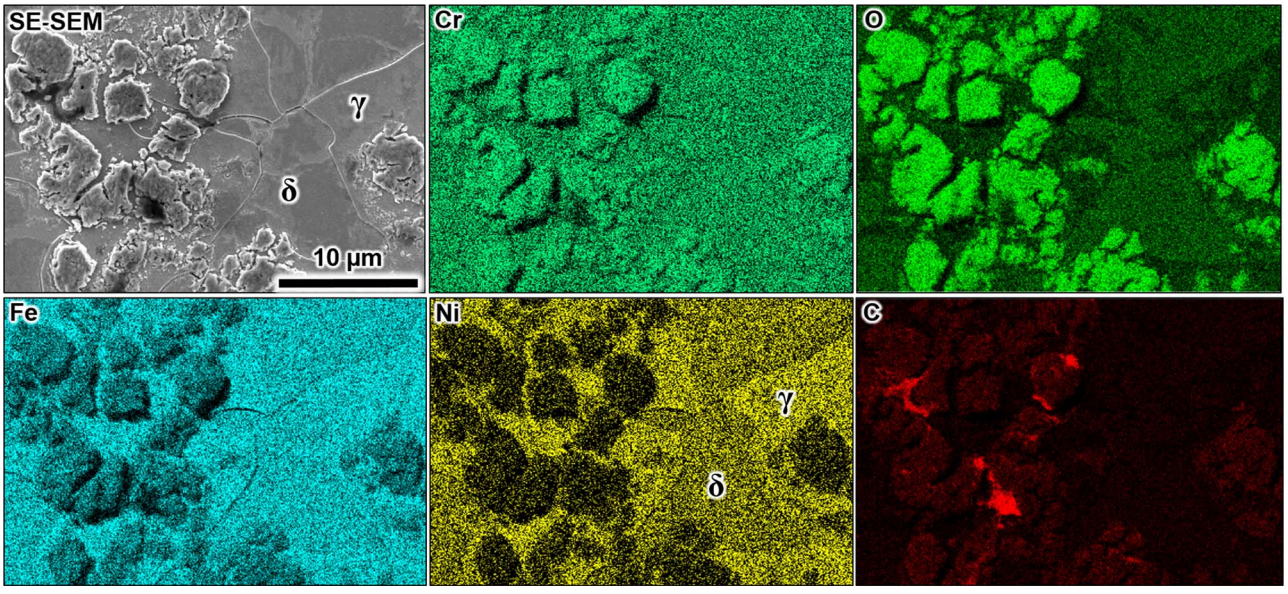

Figure 8. SEM-EDX analyses of the surface on the edge of the sample after polarization to 1400 mV in 0.1 M NaCl showing selective dissolution occurred on ferrite, apparent from Cr and Mo enrichments in the ferrite and Ni enrichment in the austenite. Mo did not show clear contrast between ferrite and austenite and is therefore not shown.

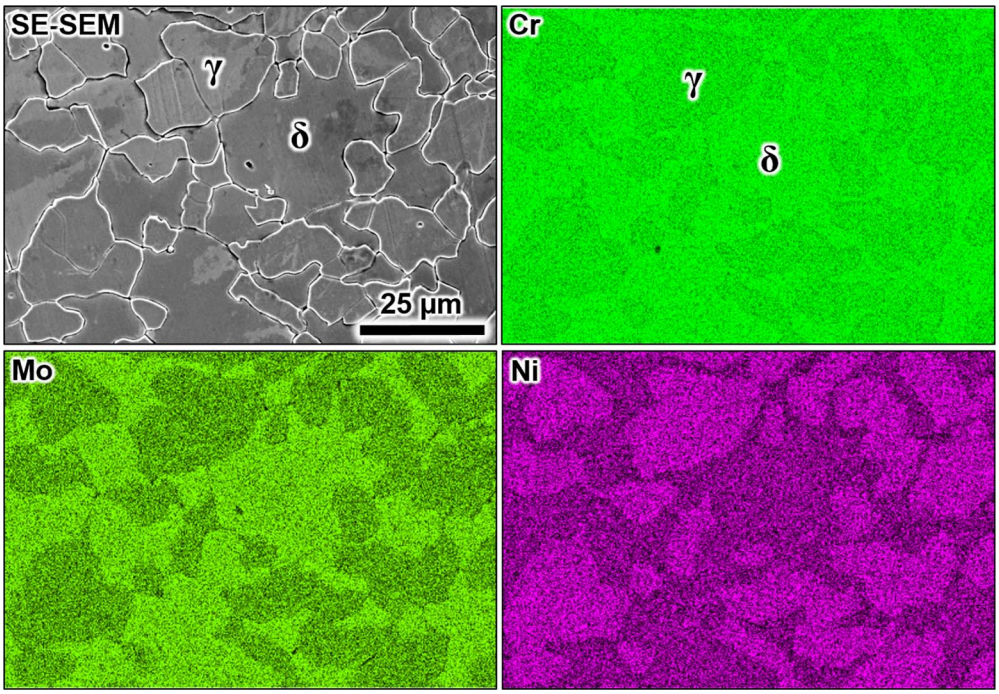

Figure 9. SEM-EDX analyses of the surface after polarization to 1400 mV in 0.1 M NaCl showing the composition of the corrosion products indicating chromium oxide. The oxides precipitates preferentially on austenitic grains (note the Ni enrichment next to the deposits indicating austenitic regions). Also note large oxide signals coming from the surface of ferritic grains indicating oxide thickening.

enriched in Cr and Mo but depleted in Ni. Interestingly, Mo had here a stronger contrast than Cr, which usually is the opposite for freshly ground/polished surfaces, indicating no or minor dissolution of Mo at this site. The site-specific dissolution behavior is likely related to locally varying pH and hence potentials/currents as well as strain/stress, which lead to different dissolution kinetics of the alloying elements. At this site, most dissolution occurred on the phase boundaries and grain boundaries (Figure 9). The Cr-contrast between the two phases showed that the surface was not homogeneous in Cr, suggesting that either both phases dissolved Cr in similar amounts or the austenite dissolved more Cr. The Ni-contrast was strong, suggesting that Ni became more enriched in the austenite and/or that ferrite dissolved Ni more readily. This also suggests that the thickness of the Ni-rich alloy surface layer varies beneath the passive film over ferrite and austenite regions.

Conclusions

Combined electrochemical and in-situ synchrotron GIXRD and XRF studies at room temperature of SAF 2507 super duplex stainless steel, mechanically ground and polished and aged for one week in ambient air, have led to following conclusions:

- Grinding and polishing resulted in strains in the surface, compressive perpendicular to the surface but most-likely tensile along the surface, affecting the crystalline structure of the passive film as well as its degradation behavior.
- The native air-formed passive oxide film formed on the sample with surface strain was mainly amorphous containing, however, some crystalline oxy-hydroxides of Cr and Fe were detected.
- The reformed oxide after transpassive dissolution due to anodic polarization beyond the transpassive breakdown potential (in 0.1 M NaCl solution) had an increased fraction of crystalline oxide/hydroxide species because of dissolution-induced strain relaxation.
- Strain in the surface layer caused enhanced susceptibility to the preferential dissolution of Fe and Cr. The propensity to the selective transpassive dissolution of the ferrite became significantly reduced due to the heavily-strained austenite, causing enhanced dissolution of the austenite. However, dissolution-induced strain relaxation in the austenite was more than that in the ferrite despite the lower dissolution of the austenite.
- The transpassive dissolution over the exposed surface was non-uniform, with the center being less active than the edge. The ferrite dissolved slightly more than the austenite in the edge area, whereas numerous micro- and nano-pits developed in austenite and ferrite grains in regions between the edge and the center.
- Strain increased the susceptibility to transpassive corrosion of the austenite thereby reducing the selective dissolution nature of the ferrite (reduced galvanic coupling), with the ferrite, however, being still the predominantly dissolving phase.

Acknowledgment

The authors are grateful for the financial support of the Swedish Research Council (Vetenskapsrådet) through the project grant no. 2015-04490 and the Sweden-Germany collaboration grant no. 2015-06092. The authors acknowledge the European Synchrotron Radiation Facility for granting access to the beamline ID03 for conducting X-ray studies.

ORCID

Cem Örnek https://orcid.org/0000-0002-3029-6493
Gary Harlow https://orcid.org/0000-0001-6644-0648
Roberto Felici https://orcid.org/0000-0001-9897-5866
Edvin Lundgren https://orcid.org/0000-0002-3692-6142
Jinshan Pan https://orcid.org/0000-0002-4431-0671

References

1. Z. Szklarska-Smialowska, Pitting Corrosion of Metals, National Association of Corrosion Engineers, Houston, Texas, USA, 1986.
2. V. Maurice and P. Marcus, Progress in corrosion science at atomic and nanometric scales, *Progress in Materials Science*, **95**, 132 (2018).

3. G. Frankel, G. Thornton, S. Street, T. Rayment, D. Williams, A. Cook, A. Davenport, S. Gibbon, D. Engelberg, C. Örnek, A. Mol, P. Marcus, D. Shoesmith, C. Wren, K. Yliniemi, G. Williams, S. Lyon, R. Lindsay, T. Hughes, J. Lutzenkirchen, S.-T. Cheng, J. Scully, S. F. Lee, R. Newman, C. Taylor, R. Springell, J. Mauzeroll, S. Virtanen, S. Heurtault, and J. Sullivan, Localised corrosion: general discussion, *Faraday Discussions*, **180**, 381 (2015).
4. V. Maurice and P. Marcus, Structure, Passivation and Localized Corrosion of Metal Surfaces, in: S.-I. Pyun and J.-W. Lee, (Eds.) *Progress in Corrosion Science and Engineering I: Progress in Corrosion Science and Engineering I*, Springer New York, New York, NY, 2010, pp. 1.
5. P. Marcus and V. Maurice, Passivity of Metals and Alloys, in: Materials Science and Technology, Wiley-VCH Verlag GmbH & Co. KGaA, 2006.
6. S. Virtanen, P. Schmuki, and H. S. Isaacs, In situ X-ray absorption near edge structure studies of mechanisms of passivity, *Electrochimica Acta*, **47**, 3117 (2002).
7. L. J. Oblonsky and M. P. Ryan, In Situ X-Ray Absorption Near-Edge Structure Study of the Active and Transpassive Dissolution of Passive Films on Ni and Ni-Cr Alloys in 0.1 M H_2SO_4, *Journal of The Electrochemical Society*, **148**, B405 (2001).
8. H. S. Isaacs, S. Virtanen, M. P. Ryan, P. Schmuki, and L. J. Oblonsky, Incorporation of Cr in the passive film on Fe from chromate solutions, *Electrochimica Acta*, **47**, 3127 (2002).
9. J. A. Bardwell, G. I. Sproule, B. MacDougall, M. J. Graham, A. J. Davenport, and H. S. Isaacs, In Situ XANES Detection of Cr(VI) in the Passive Film on Fe-26Cr, **139**, 371 (1992).
10. L. J. Oblonsky, M. P. Ryan, and H. S. Isaacs, In Situ Determination of the Composition of Surface Films Formed on Fe-Cr Alloys, **145**, 1922 (1998).
11. J. Soltis, Passivity breakdown, pit initiation and propagation of pits in metallic materials – Review, *Corrosion Science*, **90**, 5 (2015).
12. C. O. A. Olsson and D. Landolt, Passive films on stainless steels—chemistry, structure and growth, *Electrochimica Acta*, **48**, 1093 (2003).
13. V. Maurice, H. Peng, L. H. Klein, A. Seyeux, S. Zanna, and P. Marcus, Effects of molybdenum on the composition and nanoscale morphology of passivated austenitic stainless steel surfaces, *Faraday Discussions*, **180**, 151 (2015).
14. V. Vignal, H. Krawiec, O. Heintz, and D. Mainy, Passive properties of lean duplex stainless steels after long-term ageing in air studied using EBSD, AES, XPS and local electrochemical impedance spectroscopy, *Corrosion Science*, **67**, 109 (2013).
15. C.-O. A. Olsson, The influence of nitrogen and molybdenum on passive films formed on the austenoferritic stainless steel 2205 studied by AES and XPS, *Corrosion Science*, **37**, 467 (1995).
16. C. Örnek, M. Långberg, J. Evertsson, G. Harlow, W. Linpé, L. Rullik, F. Carlà, R. Felici, E. Bettini, U. Kivisäkk, E. Lundgren, and J. Pan, In-situ synchrotron GIXRD study of passive film evolution on duplex stainless steel in corrosive environment, *Corrosion Science*, **141**, 18 (2018).
17. D. D. Macdonald, Some personal adventures in passivity—A review of the point defect model for film growth, *Russian Journal of Electrochemistry*, **48**, 235 (2012).
18. D. D. Macdonald, The Point Defect Model for the Passive State, *Journal of The Electrochemical Society*, **139**, 3434 (1992).
19. N. Sato, Anodic Breakdown of Passive Films on Metals, *Journal of The Electrochemical Society*, **129**, 255 (1982).
20. P. Marcus and V. Maurice, The Structure of Passive Films on Metals and Alloys, in: M.B. Ives, J.L. Luo, and J.R. Rodda, (Eds.) *Passivity of Metals and Semiconductors*, The Electrochemical Society, Jasper Park Lodge, Canada, 1999, pp. 30.
21. J. A. Bearden and X-Ray Wavelengths, *Reviews of Modern Physics*, **39**, 78 (1967).
22. J. Seong, F. Yang, F. Scheltens, G. S. Frankel, and N. Sridhar, Influence of the Altered Surface Layer on the Corrosion of AA5083, *Surface and Interface Analysis*, **162**, C209 (2015).
23. N. Sato and G. Okamoto, Electrochemical Passivation of Metals, in: J.O.M. Bockris, B.E. Conway, E. Yeager, and R.E. White, (Eds.) *Electrochemical Materials Science*, Springer US, Boston, MA, 1981, pp. 193.
24. B. M. Sass and D. Rai, Solubility of amorphous chromium(III)-iron(III) hydroxide solid solutions, *Inorganic Chemistry*, **26**, 2228 (1987).
25. D. Kempf, V. Vignal, N. Martin, and S. Virtanen, Relationships between strain, microstructure and oxide growth at the nano- and microscale, *Surface and Interface Analysis* **40**, 43 (2008).
26. K. N. Lyon, T. J. Marrow, and S. B. Lyon, Influence of milling on the development of stress corrosion cracks in austenitic stainless steel, *Journal of Materials Processing Technology*, **218**, 32 (2015).
27. C. Örnek and D. L. Engelberg, Towards understanding the effect of deformation mode on stress corrosion cracking susceptibility of grade 2205 duplex stainless steel, *Materials Science and Engineering: A*, **666**, 269 (2016).
28. C. Örnek and D. L. Engelberg, An experimental investigation into strain and stress partitioning of duplex stainless steel using digital image correlation, X-ray diffraction and scanning Kelvin probe force microscopy, *The Journal of Strain Analysis for Engineering Design*, **51**, 207 (2016).
29. N. Pettersson, S. Wessman, M. Thuvander, P. Hedström, J. Odqvist, R. F. A. Pettersson, and S. Hertzman, Nanostructure evolution and mechanical property changes during aging of a super duplex stainless steel at 300°C, *Materials Science and Engineering: A*, **647**, 241 (2015).
30. G. Petzow, Metallographisches, Keramographisches, Plastographisches Ätzen Borntraeger, Stuttgart, 2015.
31. H. Oettel and H. Schumann, *Metallografie - Mit einer Einführung in die Keramografie, 15., revised and enlarged ed.*, Wiley-VCH, Weinheim, Germany, 2011.
32. C. Örnek and D. L. Engelberg, SKPFM measured Volta potential correlated with strain localisation in microstructure to understand corrosion susceptibility of cold-rolled grade 2205 duplex stainless steel, *Corrosion Science*, **99**, 164 (2015).
33. C. Örnek, F. Léonard, S. A. McDonald, A. Prajapati, P. J. Withers, and D. L. Engelberg, Time-dependent in situ measurement of atmospheric corrosion rates of duplex stainless steel wires, *npj Materials Degradation*, **2**, 10 (2018).
34. C. Örnek, S. Idris, P. Reccagni, and D. Engelberg, Atmospheric-Induced Stress Corrosion Cracking of Grade 2205 Duplex Stainless Steel—Effects of 475°C Embrittlement and Process Orientation, *Metals*, **6**, 167 (2016).
35. C. Örnek, X. Zhong, and D. L. Engelberg, Low-Temperature Environmentally Assisted Cracking of Grade 2205 Duplex Stainless Steel beneath a $MgCl_2$:$FeCl_3$ Salt Droplet, *Corrosion*, **72**, 384 (2015).
36. S. Aoki, K. Ito, H. Yakuwa, M. Miyasaka, and J. I. Sakai, Potential Dependence of Preferential Dissolution Behavior of a Duplex Stainless Steel in Simulated Solution inside Crevice, *Zairyo-to-Kankyo*, **60**, 363 (2011).
37. S. Aoki, H. Yakuwa, K. Mitsuhashi, and J. I. Sakai, Dissolution Behavior of α and γ Phases of a Duplex Stainless Steel in a Simulated Crevice Solution, *ECS Transactions*, **25**, 17 (2010).
38. W.-T. Tsai and J.-R. Chen, Galvanic corrosion between the constituent phases in duplex stainless steel, *Corrosion Science*, **49**, 3659 (2007).
39. J.-O. Nilsson, Super duplex stainless steels, *Materials Science and Technology*, **8**, 685 (1992).
40. C. R. Clayton and I. Olefjord, Passivity of Austenitic Stainless Steels, in: P. Marcus, (Ed.) *Corrosion Mechanisms in Theory and Practice*, CRC Press Taylor & Francis Group, Boca Raton, FL, USA, 2012, pp. 327.
41. E. Gardin, S. Zanna, A. Seyeux, A. Allion-Maurer, and P. Marcus, Comparative study of the surface oxide films on lean duplex and corresponding single phase stainless steels by XPS and ToF-SIMS, *Corrosion Science*, **143**, 403 (2018).
42. D. Ramachandran, R. Egoavil, A. Crabbe, T. Hauffman, A. Abakumov, J. Verbeeck, I. Vandendael, H. Terryn, and D. Schryvers, TEM and AES investigations of the natural surface nano-oxide layer of an AISI 316L stainless steel microfibre, *Journal of Microscopy*, **264**, 207 (2016).
43. B. Zhang, J. Wang, B. Wu, X. W. Guo, Y. J. Wang, D. Chen, Y. C. Zhang, K. Du, E. E. Oguzie, and X. L. Ma, Unmasking chloride attack on the passive film of metals, *Nature Communications*, **9**, 2559 (2018).